Second-order Kohn-Sham perturbation theory: Correlation potential for atoms in a cavity

Hong Jiang and Eberhard Engel[a)]
Center for Scientific Computing, Johann Wolfgang Goethe-Universität Frankfurt, Max-von-Laue-Straße 1, D-60438 Frankfurt am Main, Germany

(Received 30 June 2005; accepted 3 October 2005; published online 12 December 2005)

Second-order perturbation theory based on the Kohn-Sham Hamiltonian leads to an implicit density functional for the correlation energy E_c^{MP2}, which is explicitly dependent on both occupied and unoccupied Kohn-Sham single-particle orbitals and energies. The corresponding correlation potential v_c^{MP2}, which has to be evaluated by the optimized potential method, was found to be divergent in the asymptotic region of atoms, if positive-energy continuum states are included in the calculation [Facco Bonetti *et al.*, Phys. Rev. Lett. **86**, 2241 (2001)]. On the other hand, Niquet *et al.*, [J. Chem. Phys. **118**, 9504 (2003)] showed that v_c^{MP2} has the same asymptotic $-\alpha/(2r^4)$ behavior as the exact correlation potential, if the system under study has a discrete spectrum only. In this work we study v_c^{MP2} for atoms in a spherical cavity within a basis-set-free finite differences approach, ensuring a completely discrete spectrum by requiring hard-wall boundary conditions at the cavity radius. Choosing this radius sufficiently large, one can devise a numerical continuation procedure which allows to normalize v_c^{MP2} consistent with the standard choice $v_c(r\to\infty)=0$ for free atoms, without modifying the potential in the chemically relevant region. An important prerequisite for the success of this scheme is the inclusion of very high-energy virtual states. Using this technique, we have calculated v_c^{MP2} for all closed-shell and spherical open-shell atoms up to argon. One finds that v_c^{MP2} reproduces the shell structure of the exact correlation potential very well but consistently overestimates the corresponding shell oscillations. In the case of spin-polarized atoms one observes a strong interrelation between the correlation potentials of the two spin channels, which is completely absent for standard density functionals. However, our results also demonstrate that E_c^{MP2} can only serve as a first step towards the construction of a suitable implicit correlation functional: The fundamental variational instability of this functional is recovered for beryllium, for which a breakdown of the self-consistent Kohn-Sham iteration is observed. Moreover, even for those atoms for which the self-consistent iteration is stable, the results indicate that the inclusion of v_c^{MP2} in the total Kohn-Sham potential does not lead to an improvement compared to the complete neglect of the correlation potential. © *2005 American Institute of Physics*. [DOI: 10.1063/1.2128674]

I. INTRODUCTION

Density-functional theory (DFT) in the Kohn-Sham (KS) formulation[1–5] has become the primary working tool for electronic structure calculations of large systems, including biomolecules, clusters, and solids.[6] The KS-DFT method owes its tremendous success to the development of rather accurate exchange-correlation (XC) functionals $E_{\mathrm{XC}}[n]$,[3,4] most notably the generalized gradient approximation (GGA).[7] The prospects of KS-DFT as a useful predictive tool for wider applications are, however, undermined by the remaining challenges that the GGA, just as the standard local-density approximation (LDA), seems hopeless to overcome: the self-interaction problem,[8] which results in an incorrect asymptotic behavior of the XC potential, the difficulty to describe dispersion forces,[9] and the failure to treat strongly correlated systems,[10] to name a few only.

Hope for a systematic improvement of XC energy functionals beyond the current GGA forms arises from the development of the so-called third generation of DFT, in which the XC energy is an explicit functional of the KS orbitals and eigenvalues, and therefore only an implicit functional of the electron density.[11–22] The corresponding XC potential v_{XC} can be calculated by the optimized (effective) potential method (OPM), which amounts to the solution of a linear integral equation for a given set of KS states.[19,23] The incorporation of the exact exchange energy (EXX) E_x, which has the same functional form as the Hartree-Fock (HF) exchange energy but is expressed in terms of the KS orbitals, solves the long-standing self-interaction problem of the conventional XC functionals. A number of systems which cannot be correctly described by GGA functionals can now be reproduced with reasonable accuracy, most notably negative ions.[24] However, for many physical properties, the application of the exact exchange without any correlation contribution gives results which are close to those obtained from HF calculations, so that the availability of the exact E_x is only of limited use as long as no appropriate correlation functional is available. The naive combination of the exact exchange with a conventional density-based correlation functional in many cases gives less accurate results than pure GGA or even LDA

a)Electronic mail: engel@th.physik.uni-frankfurt.de

calculations, due to the lack of error cancellation between exchange and correlation, which is instrumental for the success of LDA and GGA functionals. Several semiempirical orbital-dependent correlation functionals, such as the self-interaction-corrected (SIC) LDA (Ref. 8) and the Colle-Salvetti (CS) functional,[25] have been tested with the exact E_x, but the results, though accurate for some quantities, are generally not very satisfactory.[26] One is thus bound to construct appropriate orbital-dependent forms for the correlation functional in a systematic fashion.

The most direct way for developing orbital-dependent XC functionals in a systematic form is offered by the many-body perturbation theory.[13,16–19,27–29] The basic idea is to use the KS Hamiltonian as the noninteracting reference and apply standard many-body perturbation techniques. If the result is expanded in powers of the electron-electron coupling constant e^2, the first-order term of this KS perturbation theory (KSPT) series is the exact exchange of DFT. All high-order terms constitute the correlation energy functional E_c. Due to their perturbative origin, these terms are functionals of the KS orbitals and energies.

Numerical implementation of these orbital-dependent correlation functionals is not simple, the computational demands increasing rapidly with the order of the perturbation corrections considered. Current interest focuses on the self-consistent implementation of the second-order term $E_c^{(2)}$, which, besides a minor difference due to the use of the KS reference Hamiltonian, has the same functional form as the well-known second-order Møller-Plesset (MP2) energy.[30] Early perturbative applications of $E_c^{(2)}$ showed some promising features, in particular, the van der Waals interaction can be correctly described.[9,27] Recent self-consistent implementations of $E_c^{(2)}$, utilizing local basis-set expansions of the KS orbitals and potential,[28,29] reported a clear improvement of the correlation potential over the LDA and GGA.

On the other hand, the mathematical properties of the second-order correlation potential $v_c^{(2)}$ resulting from $E_c^{(2)}$ have only become clear very recently. In Ref. 31, Facco Bonetti *et al.* found that for free atoms, $v_c^{(2)}$ is divergent in the asymptotic region of large r. In contrast to the calculations in Refs. 28 and 29, this work relied on the combination of analytical arguments with a basis-set-free numerical treatment of the KS and the OPM equation. As the origin of the unphysical behavior of $v_c^{(2)}$, the presence of unoccupied states in $E_c^{(2)}$ was identified, which is a general feature of all orbital-dependent correlation functionals derived from many-body perturbation theory. On the other hand, Niquet *et al.*[32] analyzed the asymptotic behavior of $v_c^{(2)}$ analytically within the framework of the adiabatic connection fluctuation-dissipation approach and found that $v_c^{(2)}$ has the correct $-\alpha/(2r^4)$ behavior. The underlying arguments, however, are based on the assumption that the complete KS single-particle spectrum is discrete, which is not the case for free atoms. In fact, virtual excitations into the positive-energy continuum states of free atoms are indispensable to obtain the correct correlation energy.[33] In order to resolve the apparent contradiction between Refs. 31 and 32, the solubility of the OPM equation in atomic systems has been analyzed in detail in Ref. 34. The main conclusions of this work are (1) the OPM equation is not consistent with the standard asymptotic limit $v_c^{(2)}(r\to\infty)=0$, if the spectrum contains a positive-energy continuum, consistent with Ref. 31; (2) $v_c^{(2)}$ diverges for atoms with free boundary conditions if only a finite number of unoccupied KS-Rydberg states is included in $E_c^{(2)}$; and (3) the OPM equation does allow a solution with the correct asymptotic behavior in the case of a countable spectrum (e.g., atoms in a spherical cavity with hard-wall boundary conditions), if the complete spectrum is taken into account properly in the OPM procedure, consistent with Ref. 32. The main aims of this work are (1) to demonstrate that the combination of a large spherical cavity around the atom with hard-wall boundary conditions on the surface of the cavity can serve as a practical computational scheme for the numerically exact (i.e., basis-set-free) determination of the second-order correlation potential and (2) to assess unambiguously the quality of the MP2 correlation functional by a benchmark investigation of a series of prototype atoms.

The paper is organized as follows. Section II provides the general theoretical background of implicit XC functionals. Section III describes the OPM for closed-shell spherical systems, with explicit expressions for the MP2 correlation energy and the pertinent functional derivatives. In Sec. IV, we describe the numerical approach for the solution of the OPM-MP2 equation for spherical systems and address various issues that are important for the accuracy of the correlation potential. In particular, we compare two different methods to calculate the Green's function, which constitutes the core of both the kernel and the inhomogeneity of the OPM integral equation. We investigate how the accuracy of the Green's function affects the singularity of the kernel and the cancellation of the two components of the inhomogeneity. In Sec. V, the MP2 functional is compared with the LDA and GGA by a perturbative evaluation of the corresponding correlation potentials on the basis of either the exact KS ground state[35] (for He, Be, and Ne) or the exact EXX ground state (for Li and N). In Sec. VI, the MP2 functional is applied self-consistently to all closed-shell and spherical open-shell atoms up to Ar. The performance of the MP2 functional is assessed by comparison with density-dependent XC functionals and experimental data. Section VII concludes the paper and discusses possible implications of our results for other work in the field.

II. GENERAL THEORY

A. Implicit correlation energy functionals from the Kohn-Sham perturbation theory

The most attractive feature of orbital-dependent functionals is that it is possible to construct approximate XC functionals whose accuracy can be improved in a systematic manner. One such systematic approach is the Kohn-Sham perturbation theory. The basic idea of KSPT is to use the KS auxiliary system as the noninteracting reference for a many-body perturbation treatment.[19]

The starting point of the KS-DFT formalism is the assumption that for an N-electron interacting system with ground-state density $n(\mathbf{r})$, there exists a noninteracting sys-

tem with a local potential $v_s(\mathbf{r})$ that has the same ground-state density. If it exists, the KS potential v_s is uniquely determined by the ground-state density n. Consequently, all single-particle orbitals ϕ_k and energies ε_k, satisfying the KS equation (atomic units are used through the paper)

$$\left[-\frac{1}{2}\nabla^2 + v_s(\mathbf{r})\right]\phi_k(\mathbf{r}) = \varepsilon_k \phi_k(\mathbf{r}), \tag{1}$$

are functionals of the density as well.

The KS potential defines a noninteracting N-particle Hamiltonian

$$\hat{H}_s = \hat{T} + \int d^3r \hat{n}(\mathbf{r}) v_s(\mathbf{r}), \tag{2}$$

with $\hat{T}$ being the standard kinetic-energy operator. The Hamiltonian $\hat{H}$ of the actual interacting system can then be decomposed into $\hat{H}_s$ and the interaction correction $\hat{H}_1$,

$$\hat{H}_1 = \hat{W} - \int d^3r \hat{n}(\mathbf{r}) v_{\mathrm{HXC}}(\mathbf{r}), \tag{3}$$

where $\hat{W}$ denotes the electron-electron interaction operator, and $v_{\mathrm{HXC}}(\mathbf{r}) \equiv v_H(\mathbf{r}) + v_{\mathrm{XC}}(\mathbf{r})$ represents the effective e-e interaction components in v_s [with v_H denoting the Hartree potential and $v_{\mathrm{XC}}(\mathbf{r}) = \delta E_{\mathrm{XC}}/\delta n(\mathbf{r})$ the exchange-correlation potential]. Applying the standard techniques of many-body theory, one can derive the following exact expression for E_{XC}:[17]

$$\begin{aligned} E_{\mathrm{XC}} = {} & \frac{1}{2}\int d^3r \int d^3r' \frac{e^2}{|\mathbf{r}-\mathbf{r}'|}\{\langle\Phi_0|\hat{\psi}^\dagger(\mathbf{r})\hat{\psi}^\dagger(\mathbf{r}') \\ & \times \hat{\psi}(\mathbf{r}')\hat{\psi}(\mathbf{r})|\Phi_0\rangle - n(\mathbf{r})n(\mathbf{r}')\} \\ & + \sum_{n=1}^{\infty} \frac{(-i)^n}{(n+1)!}\int_{-\infty}^{\infty} dt_1 \cdots \int_{-\infty}^{\infty} dt_n \\ & \times \langle\Phi_0|T\{\hat{H}_{1,I}(0)\hat{H}_{1,I}(t_1)\cdots\hat{H}_{1,I}(t_n)\}|\Phi_0\rangle_l, \end{aligned} \tag{4}$$

where $|\Phi_0\rangle$ is the ground state of the KS system, $\hat{H}_s|\Phi_0\rangle = E_s|\Phi_0\rangle$, $\hat{H}_{1,I}(t)$ represents $\hat{H}_1$ in the interaction picture with respect to $\hat{H}_s$, $\hat{\psi}^\dagger(\mathbf{r})$ and $\hat{\psi}(\mathbf{r})$ are field operators, and the index l indicates that only linked diagrams have to be included in the evaluation of Eq. (4) via the Feynman diagrammatic technique.

Equation (4) provides an exact expression of the XC energy as a functional of the KS orbitals and energies, which, however, is highly nonlinear due to the appearance of v_{XC} on the right-hand side of Eq. (4). In order to exploit this expression in practice, one has to transform it into a numerically accessible form. A natural choice is to expand E_{XC} and v_{XC} in powers of e^2,

$$E_{\mathrm{XC}} = \sum_{l=1}^{\infty} e^{2l} E_{\mathrm{XC}}^{(l)}[n] = E_x + E_c^{(2)} + \cdots, \tag{5}$$

$$v_{\mathrm{XC}} = \sum_{l=1}^{\infty} e^{2l} v_{\mathrm{XC}}^{(l)}[n] = v_x + v_c^{(2)} + \cdots. \tag{6}$$

Insertion of these expansions on the left- and right-hand sides of Eq. (4) yields a well-defined power series in e^2. Its lowest order [the first term of Eq. (4)] represents the exact exchange functional of DFT,

$$E_x = -\frac{1}{2}\sum_{k,l}\theta_k\theta_l \int d^3r \int d^3r' \frac{\phi_k^\dagger(\mathbf{r})\phi_l(\mathbf{r})\phi_l^\dagger(\mathbf{r}')\phi_k(\mathbf{r}')}{|\mathbf{r}-\mathbf{r}'|}. \tag{7}$$

Here θ_k characterizes the occupation of the KS level k,

$$\theta_k \equiv \theta(\varepsilon_F - \varepsilon_k) \equiv \begin{cases} 1 & \text{if } \varepsilon_k \leqslant \varepsilon_F \\ 0 & \text{otherwise,} \end{cases} \tag{8}$$

with ε_F denoting the Fermi energy (highest occupied KS orbital energy). The second-order contribution to Eq. (4) can be written as the sum of two terms,

$$E_c^{(2)} = E_c^{\mathrm{MP2}} + E_c^{\Delta\mathrm{HF}}. \tag{9}$$

E_c^{MP2} has the same form as the standard MP2 expression,[30]

$$E_c^{\mathrm{MP2}} = \frac{e^4}{2}\sum_{i,j,a,b}\theta_i\theta_j\bar{\theta}_a\bar{\theta}_b \frac{(ij\,\|\,ab)[(ab\,\|\,ij) - (ab\,\|\,ji)]}{\varepsilon_i + \varepsilon_j - \varepsilon_a - \varepsilon_b}, \tag{10}$$

where $\bar{\theta}_k \equiv 1 - \theta_k$ and

$$(ij\,\|\,ab) \equiv \int d^3r_1 \int d^3r_2 \frac{\phi_i^\dagger(\mathbf{r}_1)\phi_a(\mathbf{r}_1)\phi_j^\dagger(\mathbf{r}_2)\phi_b(\mathbf{r}_2)}{|\mathbf{r}_1 - \mathbf{r}_2|} \tag{11}$$

is a Slater integral evaluated with the KS orbitals. The second term,

$$E_c^{\Delta\mathrm{HF}} = \sum_{i,a}\theta_i\bar{\theta}_a \frac{|\langle i|v_x|a\rangle + e^2\sum_j (ij\,\|\,ja)|^2}{\varepsilon_i - \varepsilon_a}, \tag{12}$$

accounts for the fact that the present perturbation expansion is not based on the HF Hamiltonian but rather on the KS Hamiltonian. $E_c^{\Delta\mathrm{HF}}$ is well defined as soon as v_x has been determined from Eq. (7) via the OPM integral equation. However, $E_c^{\Delta\mathrm{HF}}$ is much smaller than E_c^{MP2} and even vanishes for spin-saturated two-electron systems,[19] so that we will completely focus on the MP2 term in this study.

In contrast to the exact E_x and semiempirical orbital-dependent correlation functionals such as the SIC-LDA and CS functional, E_c^{MP2} depends on both the occupied and the *unoccupied* KS orbitals and *eigenenergies*, which is a common feature of all implicit correlation functionals obtained from KSPT.

B. Exchange-correlation potential from orbital-dependent functionals

As soon as the exchange-correlation energy is an explicit functional of the KS orbitals and energies, the calculation of the functional derivative $v_{\mathrm{XC}}(\mathbf{r}) = \delta E_{\mathrm{XC}}/\delta n(\mathbf{r})$ is no longer straightforward. Instead, the XC potential has to be calcu-

lated via the OPM:[19,23] The XC potential is the solution of an integral equation, which will be called the OPM equation in the following.

Formally the OPM equation can be obtained in several different ways,[19] each of which indicates different aspects of the OPM XC potential. The simplest way to derive the OPM equation is by direct functional differentiation, relying on the chain rule. For a general implicit XC functional $E_{\mathrm{XC}}[\phi_k,\varepsilon_k]$, one obtains

$$v_{\mathrm{XC}}(\mathbf{r}) = \frac{\delta E_{\mathrm{XC}}[\phi_k,\varepsilon_k]}{\delta n(\mathbf{r})} = \int d^3r' \frac{\delta v_s(\mathbf{r}')}{\delta n(\mathbf{r})} \sum_k \left\{ \int d^3r'' \left[\frac{\delta \phi_k^\dagger(\mathbf{r}'')}{\delta v_s(\mathbf{r}')} \frac{\delta E_{\mathrm{XC}}}{\delta \phi_k^\dagger(\mathbf{r}'')} + \text{c.c.} \right] + \frac{\delta \varepsilon_k}{\delta v_s(\mathbf{r}')} \frac{\partial E_{\mathrm{XC}}}{\partial \varepsilon_k} \right\}, \tag{13}$$

where we have assumed a discrete KS spectrum. Using first-order perturbation theory, one can evaluate the ingredients of (13),

$$\frac{\delta \phi_k^\dagger(\mathbf{r})}{\delta v_s(\mathbf{r}')} = -\phi_k^\dagger(\mathbf{r}') G_k(\mathbf{r}',\mathbf{r}), \tag{14}$$

$$\frac{\delta \varepsilon_k}{\delta v_s(\mathbf{r})} = \phi_k^\dagger(\mathbf{r})\phi_k(\mathbf{r}), \tag{15}$$

with the Green's function (GF) $G_k(\mathbf{r},\mathbf{r}')$ for the kth orbital being defined as

$$G_k(\mathbf{r},\mathbf{r}') = \sum_{l\neq k} \frac{\phi_l(\mathbf{r})\phi_l^\dagger(\mathbf{r}')}{\varepsilon_l - \varepsilon_k}. \tag{16}$$

Using the fact that $\delta v_s/\delta n$ is the inverse of the static KS response function,

$$\frac{\delta n(\mathbf{r})}{\delta v_s(\mathbf{r}')} \equiv \chi_s(\mathbf{r},\mathbf{r}') = -\sum_k \theta_k \phi_k^\dagger(\mathbf{r}) G_k(\mathbf{r},\mathbf{r}')\phi_k(\mathbf{r}') + \text{c.c.}, \tag{17}$$

Eq. (13) can be inverted, which leads to the OPM integral equation, a Fredholm equation of the first kind,

$$\int d^3r' \chi_s(\mathbf{r},\mathbf{r}') v_{\mathrm{XC}}(\mathbf{r}') = Q_{\mathrm{XC}}(\mathbf{r}), \tag{18}$$

with the inhomogeneity given by

$$Q_{\mathrm{XC}}(\mathbf{r}) = \sum_k \left\{ -\int d^3\tau' \left[\phi_k^\dagger(\mathbf{r}) G_k(\mathbf{r},\mathbf{r}') \frac{\delta E_{\mathrm{XC}}}{\delta \phi_k^\dagger(\mathbf{r}')} + \text{c.c.} \right] + |\phi_k(\mathbf{r})|^2 \frac{\partial E_{\mathrm{XC}}}{\partial \varepsilon_k} \right\}. \tag{19}$$

III. DETAILED FORMULATION FOR SPHERICAL SYSTEMS

A. OPM equation for spherical systems

In this paper we aim at numerically exact results for the second-order potential of closed-shell atomic systems, embedded in a (symmetry-adapted) spherical cavity. The spherical symmetry is maintained by the density and the KS potential, so that each KS orbital can be factorized as

$$\phi_k(\mathbf{r}) \to \phi_{nlm}(\mathbf{r}) = \frac{P_{nl}(\mathbf{r})}{r} Y_{lm}(\theta,\varphi), \tag{20}$$

where n is the principal quantum number, l and m are the standard angular quantum numbers, and $Y_{lm}(\theta,\varphi)$ is a spherical harmonic. The radial wave functions P_{nl} are solutions of the radial KS equation,

$$\left[-\frac{1}{2}\left(\frac{d^2}{dr^2} - \frac{l(l+1)}{r^2} \right) + v_s(r) \right] P_{nl}(r) = \varepsilon_{nl} P_{nl}(r). \tag{21}$$

As already indicated, we assume that the complete energy spectrum is discrete, which is achieved by imposing a suitable boundary conditions at some finite radius R. The OPM equation for free atoms with continuum states involved is discussed in detail in Ref. 34. In the case of spherical systems with discrete spectrum, the OPM equation reads

$$\int_0^\infty dr' K(r,r') v_{\mathrm{XC}}(r') = Q_{\mathrm{XC}}(r). \tag{22}$$

The kernel $K(r,r')$ is the radial density response function

$$K(r,r') \equiv \frac{\delta(4\pi r^2 n(r))}{\delta v_s(r')}, \tag{23}$$

which can be calculated using the radial form of the Green's function [Eq. (16)] (for the explicit form of G_{nl} see below),

$$K(r,r') = -4\sum_{nl} \theta_{nl}(2l+1) P_{nl}(r) G_{nl}(r,r') P_{nl}(r'), \tag{24}$$

and the inhomogeneity reads

$$Q_{\mathrm{XC}}(r) = \sum_{nl} P_{nl}(r) \int_0^\infty dr' \left[-\frac{\delta E_{\mathrm{XC}}}{\delta P_{nl}(r')} \right] G_{nl}(r',r) + \sum_{nl} \frac{\partial E_{\mathrm{XC}}}{\partial \varepsilon_{nl}} P_{nl}(r)^2. \tag{25}$$

B. The Orbital Green's function

One of the most important ingredients of the OPM procedure is the Green's function [Eq. (16)], which, for spherical systems, satisfies the differential equation[15,23]

$$\left[-\frac{1}{2}\left(\frac{d^2}{dr^2} - \frac{l(l+1)}{r^2} \right) + v_s(r) - \varepsilon_{nl} \right] G_{nl}(r,r') = \delta(r-r') - P_{nl}(r)P_{nl}(r'). \tag{26}$$

There are two approaches that can be used to calculate $G_{nl}(r,r')$ in practice, the direct sum-over-states (SoS) method,

$$G_{nl}(r,r') = \sum_{n'\neq n} \frac{P_{n'l}(r)P_{n'l}(r')}{\varepsilon_{n'l} - \varepsilon_{nl}}, \tag{27}$$

and the second solution (SECSOL) method, as suggested in the original work of Talman and Shadwick.[23] This latter approach relies on the second, non-normalizable solution $Q_{nl}(r)$

of the radial KS equation for any given KS eigenvalue ε_{nl}. $Q_{nl}(r)$ is related to the normalizable solution $P_{nl}(r)$ by

$$P_{nl}(r)Q'_{nl}(r) - P'_{nl}(r)Q_{nl}(r) = 1, \tag{28}$$

where the prime indicates a differentiation with respect to r. This relation can be utilized to express the Green's function as

$$G_{nl}(r,r') = 2[Q_{nl}(r_<)P_{nl}(r_>) - P_{nl}(r)\Psi_{nl}(r') - P_{nl}(r')\Psi_{nl}(r) + C_{nl}P_{nl}(r)P_{nl}(r')], \tag{29}$$

with

$$\Psi_{nl}(r) \equiv P_{nl}(r)\int_0^r P_{nl}(r')Q_{nl}(r')dr' + Q_{nl}(r)\int_r^\infty P_{nl}(r')^2 dr', \tag{30}$$

$$C_{nl} \equiv \int_0^\infty P_{nl}(r)\Psi_{nl}(r)dr, \tag{31}$$

and $r_< \equiv \min(r,r')$ and $r_> \equiv \max(r,r')$.

One can easily verify analytically that both forms [Eqs. (27) and (29)] satisfy the differential equation (26). However, the two forms are quite different, as soon as a practical numerical realization is required. The SECSOL form can be implemented in a numerically "exact" fashion, in the sense that both $P_{nl}(r)$ and $Q_{nl}(r)$ can be calculated by the solution of the radial KS equation on a grid to any desired accuracy, at least in principle. In contrast, the accuracy of the SoS form not only depends on the accuracy of the orbitals on the grid but also on the number of states included in the sum over n' inherent in Eq. (27). Thus the SoS form is quite sensitive to the degree of completeness of the numerically available part of the KS spectrum, while the complete KS spectrum is automatically incorporated in Eq. (29) via the closure relation. The SECSOL method is also computationally more efficient than the SoS form. On the other hand, in the case of the MP2 problem, the SoS method might offer a more consistent treatment, since the calculation of E_c^{MP2} and the associated inhomogeneity will necessarily be restricted to the available part of the KS spectrum. We will therefore compare these two approaches in the next section.

C. MP2 correlation functional for spherical systems

Throughout this section, we use the abbreviation $k \equiv (n_k l_k)$ and the convention that the indices i,j represent occupied orbitals, a,b represent unoccupied orbitals, and k,l represent the general case. The MP2 energy for closed-shell systems then reads

$$E_c^{\mathrm{MP2}}[P_k,\varepsilon_l] = \sum_{i,j,a,b} (\varepsilon_i + \varepsilon_j - \varepsilon_a - \varepsilon_b)^{-1} \sum_L R_L^{ijab} \times \left[2C_{D;L}^{ijab} R_L^{ijab} + \sum_{L'} C_{X;LL'}^{ijab} R_{L'}^{ijba} \right]. \tag{32}$$

The coefficients $C_{D,L}^{ijab}$ and $C_{X,LL'}^{ijab}$ arise from angular momentum coupling.[36] In terms of the Wigner $3j$ and $6j$ symbols, they are given by

$$C_{D;L}^{ijab} = \frac{(2l_i+1)(2l_j+1)(2l_a+1)(2l_b+1)}{2L+1} \times \begin{pmatrix} l_i & l_a & L \\ 0 & 0 & 0 \end{pmatrix}^2 \begin{pmatrix} l_j & l_b & L \\ 0 & 0 & 0 \end{pmatrix}^2, \tag{33}$$

$$C_{X;LL'}^{ijab} = (2l_i+1)(2l_j+1)(2l_a+1)(2l_b+1)(-1)^{L+L'+1} \times \begin{pmatrix} l_i & l_a & L \\ 0 & 0 & 0 \end{pmatrix} \begin{pmatrix} l_j & l_b & L \\ 0 & 0 & 0 \end{pmatrix} \begin{pmatrix} l_i & l_b & L' \\ 0 & 0 & 0 \end{pmatrix} \times \begin{pmatrix} l_j & l_a & L' \\ 0 & 0 & 0 \end{pmatrix} \begin{Bmatrix} l_i & l_a & L \\ l_j & l_b & L' \end{Bmatrix}. \tag{34}$$

R_L^{ijab} is the radial Slater integral

$$R_L^{ijab} = \int_0^\infty dr \int_0^\infty dr' P_i(r)P_j(r')v_L(r,r')P_a(r)P_b(r'), \tag{35}$$

with

$$v_L(r,r') \equiv \frac{r_<^L}{r_>^{L+1}}. \tag{36}$$

From Eq. (32) one can obtain the derivatives of E_c^{MP2} with respect to the radial orbitals and eigenenergies. To simplify the notation, we first define

$$S_L^{ijab} \equiv 2C_{D;L}^{ijab}R_L^{ijab} + \sum_{L'} C_{X;LL'}^{ijab} R_{L'}^{ijba}, \tag{37}$$

$$\Delta_{ijab} \equiv \varepsilon_i + \varepsilon_j - \varepsilon_a - \varepsilon_b. \tag{38}$$

After some algebraic transformations we obtain

$$\frac{\delta E_c^{\mathrm{MP2}}}{\delta P_i(r)} = 4\sum_{jab} \Delta_{ijab}^{-1} \sum_L S_L^{ijab} v_L^{jb}(r) P_a(r), \tag{39}$$

$$\frac{\delta E_c^{\mathrm{MP2}}}{\delta P_a(r)} = 4\sum_{ijb} \Delta_{ijab}^{-1} \sum_L S_L^{ijab} v_L^{jb}(r) P_i(r), \tag{40}$$

$$\frac{\partial E_c^{\mathrm{MP2}}}{\partial \varepsilon_i} = -2\sum_{jab} \Delta_{ijab}^{-2} \sum_L S_L^{ijab} R_L^{ijab}, \tag{41}$$

$$\frac{\partial E_c^{\mathrm{MP2}}}{\partial \varepsilon_a} = 2\sum_{ijb} \Delta_{ijab}^{-2} \sum_L S_L^{ijab} R_L^{ijab}, \tag{42}$$

with

$$v_L^{kl}(r) \equiv \int_0^\infty dr' P_k(r')P_l(r')v_L(r,r'). \tag{43}$$

Using these equations, the MP2 inhomogeneity can be decomposed into one contribution resulting from the derivative with respect to P_k [first line of Eq. (19)] and a second term comprising the derivative with respect to ε_k [second line of Eq. (19)],

$$Q_c^{\mathrm{MP2}}(r) = Q_c^a(r) + Q_c^b(r), \tag{44}$$

$$Q_c^a(r) = 4\sum_{ijab} \Delta_{ijab}^{-1} \sum_L S_L^{ijab} \left[\sum_{k\neq i} \frac{P_i(r)P_k(r)}{\varepsilon_i - \varepsilon_k} R_L^{kjab} + \sum_{k\neq a} \frac{P_a(r)P_k(r)}{\varepsilon_a - \varepsilon_k} R_L^{ijkb} \right], \tag{45}$$

$$Q_c^b(r) = 2\sum_{ijab} \Delta_{ijab}^{-2} \sum_L S_L^{ijab} R_L^{ijab} [P_a(r)^2 - P_i(r)^2]. \tag{46}$$

Due to the orthonormality of the radial orbitals, Q_c^a and Q_c^b separately satisfy the sum rule

$$\int_0^\infty Q_c^a(r)dr = \int_0^\infty Q_c^b(r)dr = 0. \tag{47}$$

IV. NUMERICAL METHOD FOR THE MP2-OPM EQUATION

The numerical solution of the OPM equation is not trivial for the exact exchange[21] and becomes even more involved in the case of E_c^{MP2}. The MP2 functional has been implemented by Grabowski *et al.*[28] as well as Mori-Sanchez *et al.*[29] by representing the correlation potential in terms of a linear combination of atomic orbitals (LCAO) (Gaussian-type basis set). The LCAO method has the advantage of general applicability to atomic and molecular systems. On the other hand, the results obtained from the LCAO method now depend on the form and size of the basis set through both the orbitals and the potential, which introduces some uncertainty: While the role and accuracy of basis sets for the orbitals have been studied for decades and are thus well established, the same is not true for the correlation potential. For a definitive assessment of the performance of the MP2 functional thus a numerically exact approach is desirable. In this section we introduce such a basis-set-free, numerically exact approach which allows the solution of the OPM equation [Eq. (22)] for MP2-type functionals.

A. Numerical procedures

The radial KS equation is solved using the Numerov method with the Froese-Fischer fourth-order deferred difference correction.[37] A mixed logarithmic and linear mesh $\rho=\log(r)+r$ is used with an equidistant grid spacing of the ρ mesh. For the number of mesh points, which controls the accuracy of the KS orbitals and all quantities derived from them, a value of 3200 has been used. For a given KS potential, we calculate the radial KS orbitals with the principal quantum number n up to $n_{\max}$ and angular quantum number l up to $l_{\max}$. Unless stated explicitly, all results presented in this paper were obtained with $l_{\max}=6$ and $n_{\max}=300$, which correspond to an eigenenergy of roughly 1100 hartree for a cavity radius of 20 bohrs. The orbitals are then used to evaluate the Green's functions, the kernel, and the components of the inhomogeneity. Replacing the integral in Eq. (22) by a Riemann sum over the equidistant ρ mesh, the original integral equation is transformed into a set of inhomogeneous linear equations. This set is solved by either standard linear equation solvers or the singular-value decomposition (SVD) method.[38] The latter is not only suitable for the solution of linear equations with a singular coefficient matrix but also provides a clear diagnosis of the nature of the problem under study.[38] The direct solution of the OPM equation as a set of linear equations is contaminated by numerical noise which results from the singularity of the kernel and from the inaccuracy of the inhomogeneity. The noise can be eliminated by a suitable post-treatment based on physical considerations (see below).

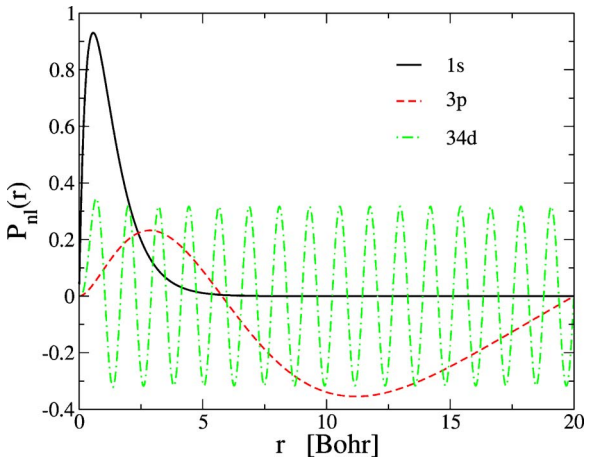

FIG. 1. (Color online) Radial orbitals of He atom in a spherical cavity of 20.0 bohr radius, applying hard-wall boundary conditions.

B. Atoms with hard-wall boundary condition

In order to avoid the difficulties associated with continuum states[34] but nevertheless simulate the free atom as well as possible, we impose hard-wall boundary conditions at some large radius R when solving Eq. (21) for a given v_s: We set all radial wave functions to zero at and beyond $r=R$ (and normalize them to 1 inside the sphere of radius R). The value of R is chosen so that all occupied orbitals vanish before they reach the hard wall and all properties under study are independent of the value of R. Figure 1 shows some typical wave functions of the He atom for a box radius of $R=20.0$ bohrs. The occupied and lowest unoccupied orbitals are extremely close to those of the free helium, while unoccupied orbitals with positive eigenvalues tend to the oscillating states typical for systems with hard-wall boundary conditions. The effect of the hard-wall boundary condition is further demonstrated in Table I, in which the orbital energies of He calculated from the exact KS potential with boundary at $R=20.0$ bohrs and $R=30.0$ bohrs are compared with the eigenvalues of the free atom. Already for $R=20.0$ bohrs, the energies for $1s$, $2s$, and $2p$ agree with the free-atom values up to 0.01 mhartree.

As a further check of the insensitivity of the results to the hard wall, Fig. 2 shows the convergence of the total MP2 correlation energy with respect to the highest shell $n_{\max}$ included in E_c^{MP2} for both $R=20.0$ bohrs and $R=30.0$ bohrs (all calculations are based on the exact KS orbitals and eigenvalues). The MP2 energies for the two different box radii converge to the same value, −48.2 mhartree, which agrees very well with the result obtained for a free He atom with con-

TABLE I. KS eigenvalues (in hartree) of He obtained for different boundary conditions (R in bohr).

	Atom in box		
Orbital	$R=20.0$	$R=30.0$	Free atom
$1s$	−0.903 73	−0.903 73	−0.903 73
$2s$	−0.157 73	−0.157 73	−0.157 73
$2p$	−0.126 56	−0.126 57	−0.126 57
$3s$	−0.061 95	−0.064 47	−0.064 50
$3p$	−0.052 35	−0.056 02	−0.056 09
$3d$	−0.053 99	−0.055 55	−0.055 58
$4s$	0.000 07	−0.031 10	−0.034 90

tinuum states.[19] This result is consistent with the fact that the MP2 energy is a ground-state density functional, which should be independent of R, as long as R falls outside the chemically relevant region. In practice, the number of virtual orbitals required to achieve the same accuracy increases with increasing R, as it is controlled by the eigenvalue of the highest virtual state included in E_c^{MP2}. Unless stated explicitly, $R=20.0$ bohrs is employed in this work.

After the KS potential is calculated with this boundary condition, it is straightforward to extend the potential to values beyond R, so that other physical quantities, e.g., the full Rydberg series, can be evaluated with the required free boundary condition. This is legitimate because the potential in the asymptotic region is exactly known.

C. The Green's function and kernel

Figure 3 compares the Green's functions for the $1s$ orbital obtained from the two methods introduced in Sec. III B. The GF from the SoS method reproduces the main features of the exact GF quite well, but the differences are significant even if a very large number of unoccupied levels is included. The accuracy of the GF directly affects (1) the singularity of the kernel and (2) the cancellation between Q_c^a and Q_c^b. We first investigate the former effect.

Figure 4(a) shows the diagonal of the kernel $K(r,r')$ resulting from the two methods. As for the GF, the kernel

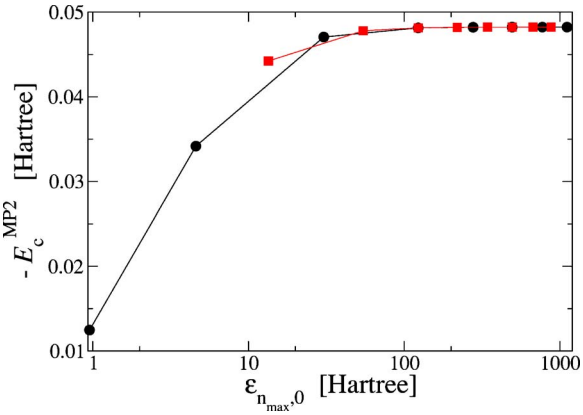

FIG. 2. (Color online) Convergence of total MP2 correlation energy of He with respect to highest shell $n_{\max}$ included in the sums over unoccupied states for two different cavity radii, $R=20.0$ bohrs (circles) and 30.0 bohrs (squares).

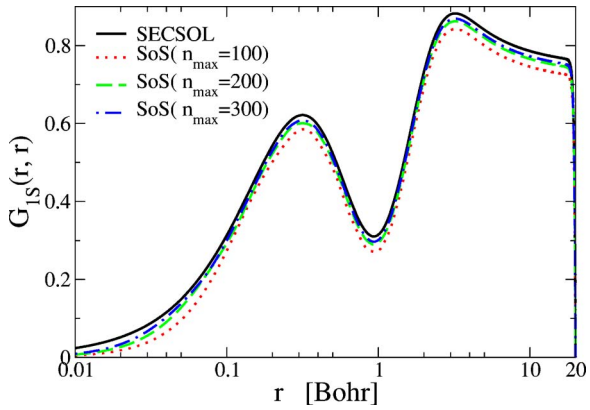

FIG. 3. (Color online) Diagonal elements of the Green's function for the $1s$ orbital of He, calculated via the SECSOL (solid) and the SoS methods for different $n_{\max}$ [100 (dot), 200 (dash), and 300 (dash dot)].

calculated by the SoS method reproduces the main features of the exact K, but the differences are not negligible even for $n_{\max}=300$. This is true, in particular, in the small-r region, as shown in the inset of Fig. 4(a). The analytic properties of the kernel calculated from the two approaches differ even more dramatically: The SoS kernel is much more singular than the SECSOL variant. Figure 4(b) illustrates this statement by displaying the singular values of the kernel obtained from the SVD procedure. The singular values of the exact kernel form a smoothly decreasing spectrum. In contrast, most of the singular values of the SoS kernel are close to zero, indicating that the corresponding linear equation is highly singular. In

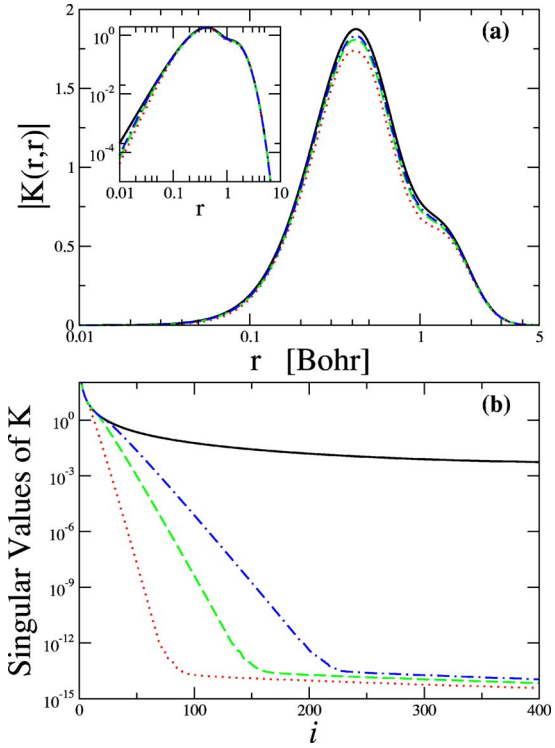

FIG. 4. (Color online) Upper panel: the diagonal elements of the kernel $K(r,r)$ calculated using the second solution method (solid) and the sum-over-states method with $n_{\max}$ being 100 (dot), 200 (dash), and 300 (dash dot) for He with $R=20$ bohrs; the inset shows the same quantities on a logarithmic scale. Lower panel: singular values of the corresponding kernel obtained from the single-value decomposition. i goes through the mesh points.

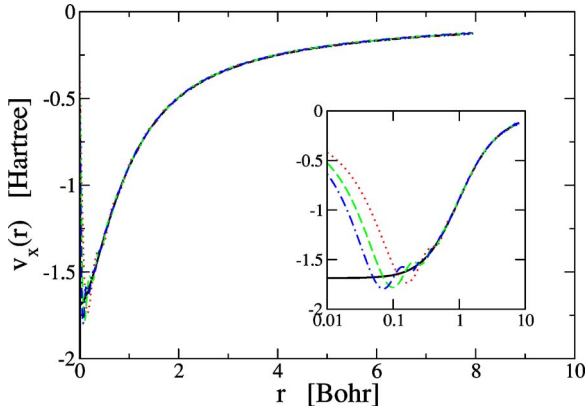

FIG. 5. (Color online) EXX exchange potential of He atom in box with $R=20$ bohrs: Comparison of potentials obtained by SECSOL (solid) and SoS methods for different values of $n_{\max}$ [100 (dot), 200 (dash), and 300 (dash dot)]. Inset: the same plot on log-scaled x axis.

practice, we found that the OPM equation with the exact kernel can be solved directly by standard linear equation solvers, while for the SoS kernel the SVD treatment is necessary.

The consequences of the two different methods for the calculation of the GF are further examined in Fig. 5, which shows the exchange potentials obtained by the two methods. The error in the v_x from the SoS method is most pronounced in the small-r region. We just remark that the effect of the inaccuracy of the SoS kernel is even more dramatic in the case of the MP2 correlation potential: Using the SoS kernel with $n_{\max} \leqslant 300$ leads to a qualitatively incorrect potential over the whole range of r values taken into account. For that reason we consistently use the SECSOL scheme for the evaluation of $K(r,r')$ for all subsequent results.

D. Cancellation in the MP2 inhomogeneity

In order to obtain a correlation potential with the correct asymptotic behavior $v_c(r\to\infty)=0$, the inhomogeneity Q_c of the free atoms has to decay to zero as fast as Q_x, so that the ratio Q_c/Q_x becomes constant as $r\to\infty$.[31,34] While this result is not directly applicable to the presently studied systems in a cavity, one would nevertheless expect that there exists a range of semiasymptotic r values (1 bohr$\ll r<R$) for which Q_c/Q_x is roughly constant (of course, the hard-wall boundary condition at $r=R$ will affect Q_c/Q_x for all $r\approx R$).

Figure 6 shows the MP2 inhomogeneity Q_c^{MP2} and its components Q_c^a and Q_c^b for two different R values. The most striking feature is that both Q_c^a and Q_c^b become almost constant in the large-r region but with opposite signs. The magnitude of this constant decreases as the box radius R increases, and a scaling of $1/R$ can be extracted from the data. This confirms the result of an analytical investigation of the asymptotic behavior of the MP2 correlation potential.[34] It is obvious from Fig. 6(a) that in the semiasymptotic regime, a cancellation between Q_c^a and Q_c^b occurs which lets the total Q_c^{MP2} nearly vanish. We also note that, although the constant approached by Q_c^a and Q_c^b depends on R, the total Q_c is almost identical in the chemically relevant region. As demonstrated in Ref. 34, an exact cancellation between Q_c^a and

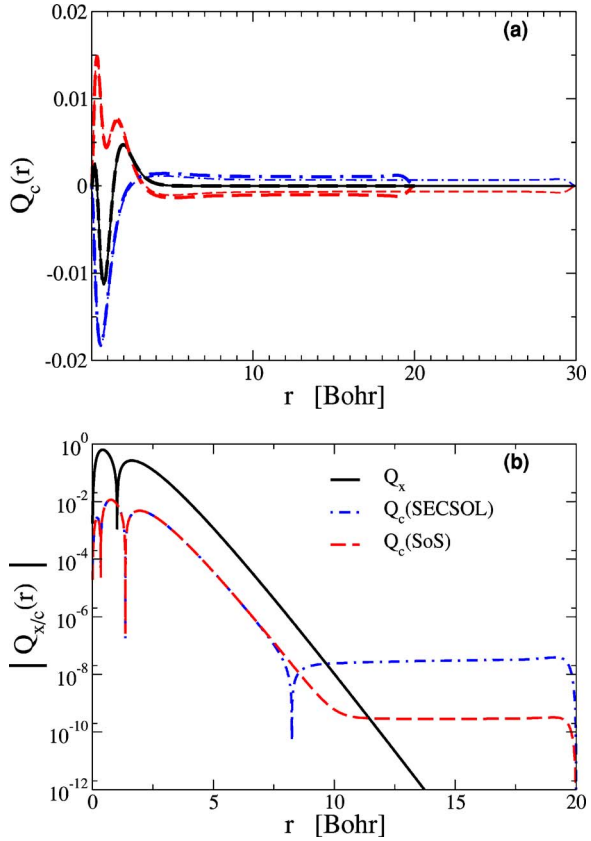

FIG. 6. (Color online) (a) Q_c^a (dash), Q_c^b (dash dot), and Q_c^{MP2} (solid) for $R=20.0$ bohrs (thick lines) and $R=30.0$ bohrs (thin lines). (b) Q_c (in absolute values) calculated using the SoS (dash) and SECSOL (dash dot) methods; for comparison Q_x also is plotted.

Q_c^b is extremely difficult to achieve, as it requires the inclusion of the complete KS spectrum. For any finite number of KS orbitals included in Q_c^a and Q_c^b, the cancellation breaks down beyond a certain critical r value, which depends on $n_{\max}$. In addition, the numerical accuracy of Q_c^a and Q_c^b is limited by the number of mesh points $I_{\max}$ used for the calculation of the highest energy states. As a consequence Q_c becomes saturated beyond some saturation radius $r^*<R$ [see Fig. 6(b)].

The computation of Q_c involves the Green's function, which can be calculated by either the SoS or the SECSOL method. The SECSOL method gives numerically exact Green's functions. However, in terms of consistency, the SoS method is expected to be more appropriate for the calculation of Q_c, as it ensures that the same finite Hilbert space is used for the calculation of all ingredients of Q_c. Figure 6(b) shows the Q_c obtained by the two methods, which demonstrates clearly that the SoS method leads to a significantly better cancellation between Q_c^a and Q_c^b: The saturation value of Q_c is almost two orders of magnitude smaller than in the case of the SECSOL approach, and the saturation radius r^* is larger. Moreover, the fictitious structure around r^* observed in the Q_c originating from the SECSOL method disappears. In the following we therefore always use the Q_c resulting from the SoS approach.

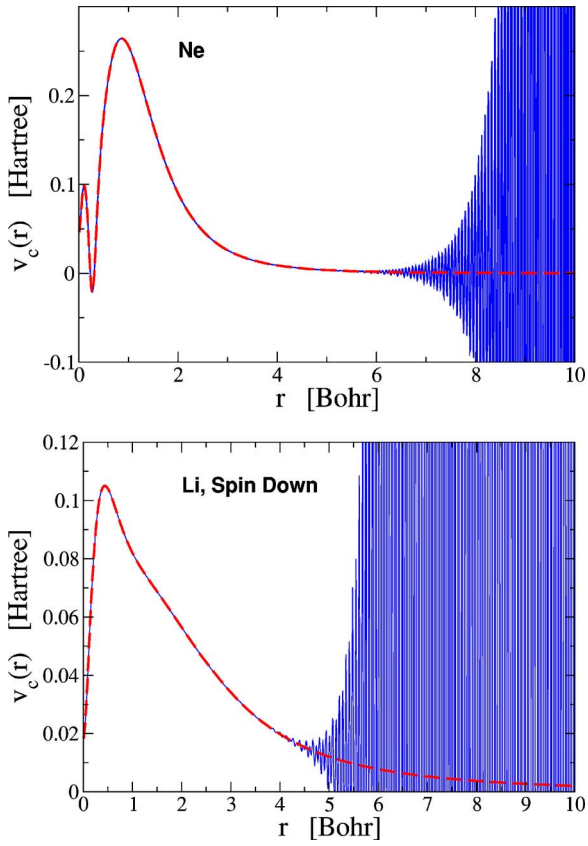

FIG. 7. (Color online) The MP2 correlation potential before (solid) and after (dashed) the post-treatment for neon (upper) and the minority-spin channel of lithium (lower). The unmodified solution of the OPM equation, $v_c^{(0)}$, has already been shifted by the constant C_0 that is determined by the generalized least-squares-fitting technique, in order to allow for a direct comparison with the final v_c^{MP2}.

E. Post-treatment of the MP2 correlation potential

The incompleteness of the SoS calculation of the inhomogeneity and the inaccuracy due to the finite number of grid points lead to numerical noise in the direct solution of the OPM equation on the grid, denoted as $v_c^{(0)}$, especially in the large-r region. A post-treatment of $v_c^{(0)}$, which removes the numerical noise and renormalizes the potential to the correct asymptotic limit $v_c^{\mathrm{MP2}}(r\to\infty)=0$, is necessary.

Figure 7 shows the unmodified $v_c^{(0)}$ for neon, normalized such that it coincides with the final v_c^{MP2} for small and medium r. Three spatial regions can be distinguished: For $r<5$ bohrs, which is the region relevant for ground-state properties, $v_c^{(0)}$ is smooth and clean. In the large-r region, $r>7.0$ bohrs, the oscillatory structure resulting from the incomplete SoS becomes dominant. In the intermediate region, though the noise is significant, the mean value of $v_c^{(0)}$ decays smoothly to a constant, apparently following an inverse power law. If $v_c^{(0)}$ was already very close to a constant at $r=5$ bohrs, one could simply extend the numerical results for $r<5$ bohrs to larger-r values by setting $v_c^{(0)}(r>5\ \mathrm{bohrs})=0$. Unfortunately, this is not the case, so that the noisy results in the intermediate region have to be used for the extension of $v_c^{(0)}$. The most obvious concept for an extension would be a least-squares fitting (LSF) to the correct asymptotic decay $-\alpha/(2r^4)$, thus determining α. However, in the fitting region, v_c^{MP2} has not yet approached its exact asymptotic form. We therefore use a more general fitting formula,

$$v_c^{\mathrm{LSF}}(r)=C_0+\sum_{n=3}^{5}\frac{C_n}{r^n}, \tag{48}$$

allowing for more freedom. Moreover, rather than using the standard LSF method, we utilize a generalized least-squares-fitting technique, in which the fit coefficients C_n are determined by minimizing the quantity

$$W[\{C_n\}]=\sum_i [v_c^{(0)}(r_i)-v_c^{\mathrm{LSF}}(r_i)]^2+\lambda\int_R^\infty\left[\sum_{n=3}^{5}\frac{C_n}{r^n}\right]^2 dr, \tag{49}$$

with r_i going through all mesh points in the fitting region. The first term in Eq. (49) is the standard LSF error function. The second term is introduced to constrain the behavior of the fitting function in the asymptotic region, i.e., to minimize the deviation of v_c^{LSF} from zero in the truly asymptotic regime (outside the cavity). λ is a weight factor that can be used to adjust the relative importance of the second term. In practice, $\lambda=1$ works well, and the results are actually not sensitive to the variation of λ.

Since the fitting is applied outside the physically relevant region, the most important quantity to be determined in this post-treatment procedure is the constant C_0. This constant is therefore an ideal measure of the uncertainty introduced by the post-treatment: Of course, including different powers of r in Eq. (48) or changing either the fitting range or λ can affect the value of C_0. In most systems the uncertainty in C_0 is about 0.001 hartree, as has been tested by substantial variation of the critical parameters. In the worst case observed, the minority-spin channel of lithium [see Fig. 7 (lower panel)], the uncertainty is of the order of 0.01 hartree. Since the dominant contribution to v_{XC} is provided by the exchange potential, which is of the order of 0.1–0.2 hartree in the relevant region, this uncertainty of C_0 is negligible for all practical purposes. It seems worthwhile to emphasize that the uncertainty in C_0 only affects the absolute values of the KS orbitals energies and is therefore irrelevant for most physical quantities of interest. As demonstrated in Fig. 7, the present fitting strategy can remove the numerical noise and renormalize v_c^{MP2} in a rather reliable way.

V. PERTURBATIVE CALCULATIONS OF THE MP2 CORRELATION POTENTIAL

The first step of any analysis of an approximate density functional is a comparison with suitable reference results. In the first part of this section, we thus investigate v_c^{MP2} for the spin-saturated systems of helium (He), beryllium (Be), and neon (Ne), for which exact reference potentials are available from accurate quantum Monte Carlo calculations.[35] For an unambiguous comparison v_c^{MP2} is evaluated with the exact KS orbitals obtained from the Monte Carlo-based KS potentials as input, so that the results correspond to the insertion of the exact ground-state densities of the systems considered into the MP2 functional. Compared to the self-consistent

MP2 potentials, this has the advantage that all functionals are evaluated with the same density, so that the properties of the approximations themselves are directly visible (this procedure is a common practice—see, e.g., Ref. 39). In the second part of this section, the spin-polarized atoms of lithium and nitrogen are considered, for which also rather accurate reference potentials have been published by Chen *et al.* in Ref. 40.

A. MP2 correlation potential for closed-shell atoms

The MP2 correlation potentials for He, Be, and Ne resulting from the combination of the exact KS orbitals and eigenenergies with hard-wall boundary conditions at $R=20$ bohrs are compared with the VWN-LDA,[41] LYP-GGA,[42] PBE-GGA,[43] and the exact v_c (Ref. 35) in Fig. 8. As is obvious from the plots, the LDA correlation potential is essentially featureless, while both the LYP- and the PBE-GGA produce an unphysical structure in the correlation potential. In contrast, v_c^{MP2} reproduces the shell structure of the exact v_c quite well. v_c^{MP2} also shows the well-known feature[44] that in the large-r region, the true v_c approaches zero from above for He and Ne but from below for Be. On the other hand, the MP2 potentials consistently overestimate the amplitudes of the shell oscillations in the exact v_c. This result is consistent with the fact that E_c^{MP2} substantially overestimates the atomic correlation energies.[19] Nevertheless, in view of the complete failure of the LDA and GGA in reproducing the shell structure, the results for v_c^{MP2} indicate a breakthrough.

B. MP2 correlation potential for spin-polarized atoms

The MP2 correlation functional formulated in Sec. III can be easily extended to spin-polarized systems. Compared to closed-shell systems, the spin-dependent correlation potential is much less well studied.[40,45] To date, no exact Monte Carlo results comparable to those for unpolarized atoms are available. Fortunately, quite accurate spin dependent reference results have been generated on the basis of spin densities resulting from configuration-interaction (CI) calculations.[40] As the corresponding total KS potentials are not available to us, we base our analysis of v_c^{MP2} for lithium and nitrogen on the orbitals and eigenvalues obtained by self-consistent EXX calculations (in Sec. VI B the sensitivity of v_c^{MP2} to the input density is studied). The results, together with those from the VWN-LDA (Ref. 41) and the PBE-GGA are presented in Fig. 9. The spin-dependent v_c^{MP2} agrees very well with the CI-based v_c in Ref. 40. In the case of the lithium atom, the MP2 correlation potential for the majority-spin channel (spin up) $v_{c\uparrow}^{\mathrm{MP2}}$ is mainly attractive, while the minority-spin correlation potential $v_{c\downarrow}^{\mathrm{MP2}}$ is repulsive. For the nitrogen atom the signs of the MP2 correlation potential in the two spin channels are inverted. On the other hand, the behavior of the conventional density functionals is similar to that observed for unpolarized atoms.

Comparing Figs. 8 and 9, one recognizes an obvious similarity between $v_{c\downarrow}^{\mathrm{MP2}}$ of Li and v_c^{MP2} of He, which can be explained by the fact that, except for the difference in the spin degeneracy, both potentials correspond to the $1s^1$ electron configuration. For the same reason, $v_{c\uparrow}^{\mathrm{MP2}}$ of N is quite similar to v_c^{MP2} of Ne, where the underlying electron configuration is $1s^1 2s^1 2p^3$. These observations seem to suggest that $v_{c\sigma}$ is dominated by the interaction of electrons with like spin. However, this picture can no longer be kept up for $v_{c\uparrow}^{\mathrm{MP2}}$(Li), v_c^{MP2}(Be), and $v_{c\downarrow}^{\mathrm{MP2}}$(N), all of which correspond to the $1s^1 2s^1$ configuration. Although the basic shell structure of the spin density under investigation is still the same, i.e., one finds two peaks corresponding to the two occupied shells, the shapes of the correlation potentials are quite different: The second peak is barely observable in $v_{c\uparrow}^{\mathrm{MP2}}$(Li),

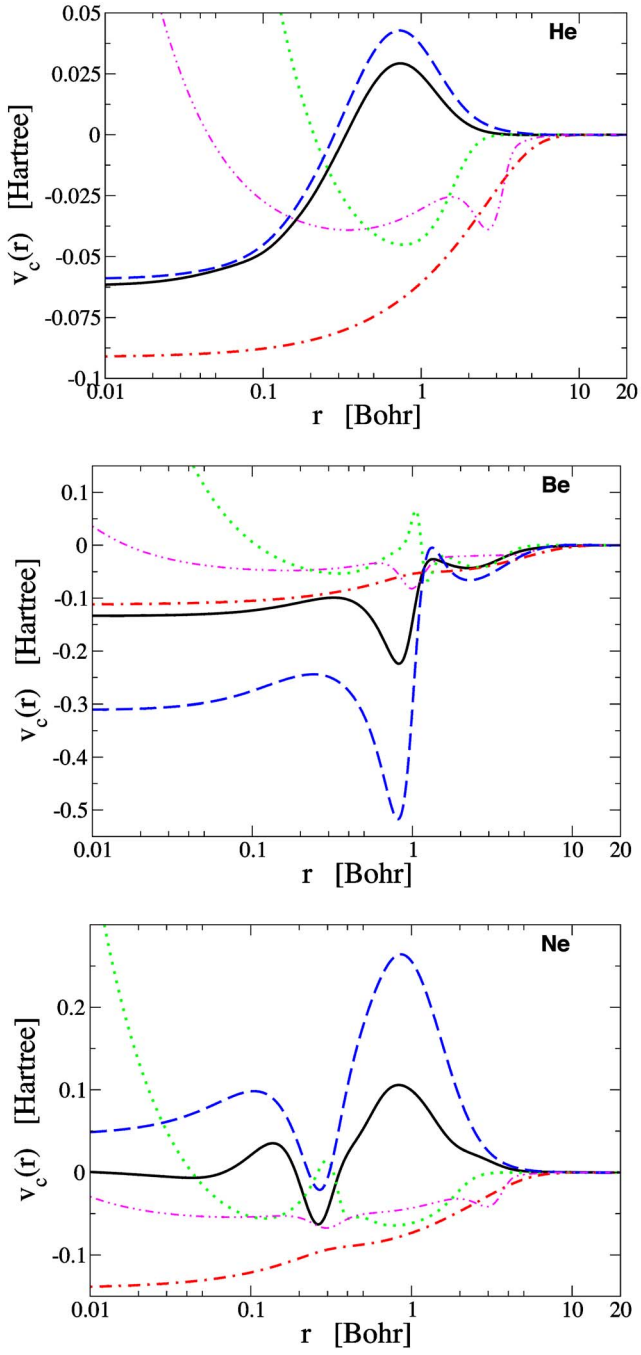

FIG. 8. (Color online) Correlation potentials corresponding to the exact ground-state densities: MP2 (long dash), VWN (dash dot), LYP (dot-dot dash), and PBE (dot), compared to exact correlation potentials (solid) for He (upper), Be (middle), and Ne (lower).

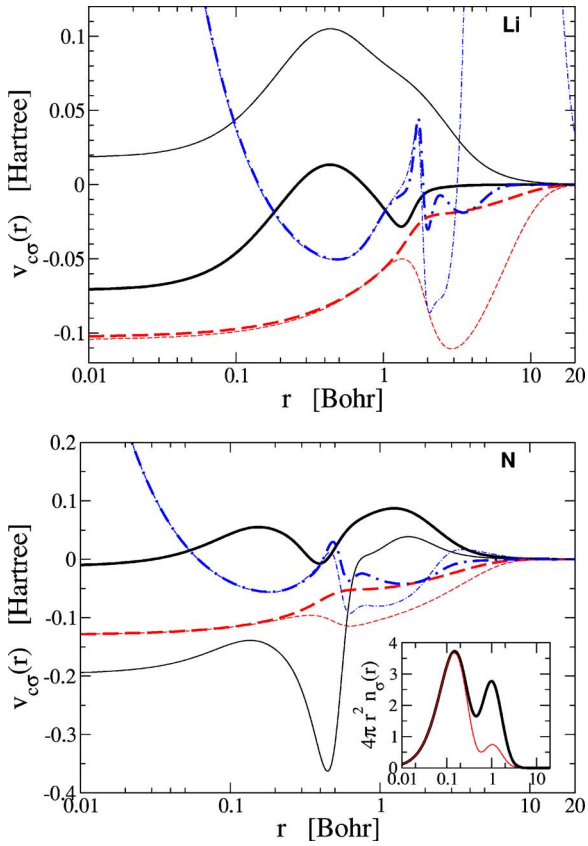

FIG. 9. (Color online) Spin-up (thick lines) and spin-down (thin lines) correlation potentials of lithium (upper panel) and nitrogen (lower panel) based on self-consistent EXX densities: MP2 (solid) vs VWN-LDA (dash) and PBE GGA (dash dot). The inset of the lower panel shows the radial spin densities of N obtained by the self-consistent EXX calculation.

much stronger in v_c^{MP2}(Be), and even becomes positive in $v_{c\downarrow}^{\mathrm{MP2}}$(N), so that the latter potential approaches zero from above in the large-r region. The variation of the strength of the second peak seems to be correlated with the change of the number of electrons in the opposite spin channel, which is 1 for Li, 2 for Be, and 5 for N. The dependence of $v_{c\sigma}$ on both the spin-up and the spin-down densities is thus obvious.

These features indicate that there are strong interrelations between the correlation potentials of the two spin channels, which are completely absent in the spin-dependent LDA and erroneously represented by various versions of the GGA. Further exploration of this aspect of the correlation functionals in spin-polarized systems may provide insight that will be useful for the development of more accurate approximate functionals.

VI. SELF-CONSISTENT CALCULATION OF THE MP2 CORRELATION POTENTIAL

The next issue to be addressed is how the MP2 functional works when employed self-consistently (SC). This issue is particularly important in the case of the MP2 functional, as inspection of Eq. (10) shows that the MP2 energy is unbounded from below, as the gap between the highest occupied molecular orbital (HOMO) and lowest unoccupied molecular orbital (LUMO) may shrink to zero. This unboundedness leads to unphysical results even if E_c^{MP2} is only applied perturbatively. For instance, N_2 is found to be unbound.[19] It is obvious that a variational minimization of the total energy with the MP2 correlation without any constraint on the orbitals is doomed to fail due to the unboundedness of the MP2 energy. On the other hand, the KS orbitals and energies correspond to a local effective potential, which introduces some constraints on the HOMO-LUMO gap. The variational instability of the MP2 expression is thus no longer obvious and can depend strongly on the particular properties of the system under consideration. We have performed self-consistent calculations with the combination of the exact exchange and MP2 correlation, denoted as EXX-MP2, for all closed-shell and spherical open-shell (with half-filled valence shell) atoms up to argon. Convergence is easily attained for all these atomic systems except for Be, which is studied separatly in Sec. VI C.

TABLE II. Total ground-state energies ($-E_{\mathrm{tot}}$ in hartree) of closed-shell and spherical open-shell atoms obtained by self-consistent calculations with different XC functionals. The last row provides the mean absolute errors (MAE) with respect to the experimental data.

Atom	EXX-MP2	VWN	BLYP	PBE	Expt.[a]
He	2.9099	2.8348	2.9071	2.8929	2.904
Li	7.4819	7.3440	7.4827	7.4622	7.479
Be	14.6965[b]	14.4472	14.6615	14.6299	14.667
N	54.6216	54.1368	54.5932	54.5357	54.590
Ne	129.0265	128.2335	128.9730	128.8664	128.937
Na	162.3195	161.4476	162.2927	162.1727	162.257
Mg	200.1286	199.1394	200.0926	199.9551	200.059
P	341.3382	340.0058	341.2779	341.1156	341.272
Ar	527.6608	525.9462	527.5510	527.3461	527.604
MAE	0.046	0.693	0.020	0.088	

[a]Experimental data including the Lamb shift corrections taken from Ref. 4.
[b]From perturbative calculation based on the EXX density.

A. Total energy and ionization potentials

Tables II and III list the total energies and ionization potentials obtained from self-consistent calculations with the EXX-MP2, EXX, VWN LDA,[41] BLYP (Becke88 exchange[46] plus LYP correlation[42]), and PBE[43] XC functionals in comparison to the corresponding experimental data. Table II shows that, in terms of the total energy, the MP2 functional is more accurate than the first-principles PBE functional but still less accurate than the semiempirical BLYP GGA. The ionization potential, as calculated from the HOMO eigenvalue of the neutral atom, is more sensitive to the accuracy of the XC potential than the total energy, especially to its asymptotic behavior. All conventional LDA and GGA functionals significantly underestimate the ionization potentials—as is well known, the GGA functionals do not show any improvement over the LDA. On the other hand, the ionization potentials calculated from the EXX and EXX-MP2 functionals are much more accurate, their average errors being one order of magnitude smaller than those of the LDA or GGA. This is mainly due to the correct asymptotic behavior of the exact v_x. The most remarkable feature in these data, however, is the fact that the EXX-MP2 ionization

TABLE III. Ionization potentials (in hartree) obtained from the HOMO eigenenergy of the neutral atoms resulting from self-consistent calculations with different XC functionals. The last row provides the mean absolute errors with respect to the experimental data.

Atom	EXX-MP2	EXX	VWN	BLYP	PBE	Expt.[a]
He	0.893	0.918	0.570	0.585	0.579	0.903
Li	0.198	0.196	0.116	0.111	0.119	0.198
Be	0.367[b]	0.309	0.206	0.201	0.206	0.343
N	0.499	0.571	0.309	0.297	0.307	0.534
Ne	0.656	0.851	0.498	0.491	0.491	0.792
Na	0.191	0.182	0.113	0.106	0.113	0.189
Mg	0.305	0.253	0.175	0.168	0.173	0.281
P	0.385	0.392	0.231	0.219	0.233	0.385
Ar	0.557	0.591	0.382	0.373	0.378	0.579
MAE	0.028	0.022	0.178	0.184	0.178	

[a]Experimental data taken from Ref. 4.
[b]From perturbative calculation based on the EXX density.

potentials are somewhat less accurate than the EXX results, indicating that inclusion of v_c^{MP2} does not improve the total KS potential.

B. Role of self-consistency

Let us therefore analyze the effect of self-consistency in more detail. In the first step, the self-consistent v_c^{MP2} for neon is compared with the perturbative potentials resulting from the EXX and the exact KS orbitals in Fig. 10. The first point to be noted in this figure is the close agreement of the two perturbative potentials. This implies that the self-consistent EXX density is quite close to the exact ground-state density, which confirms the use of EXX orbitals for the evaluation of v_c^{MP2} for lithium and nitrogen in Sec. V B. On the other hand, the self-consistent EXX-MP2 density obviously differs more from the exact density than its EXX counterpart, which requires an explanation. We have already seen in Fig. 8 that, for a fixed, given density, v_c^{MP2} overestimates the shell oscillations in the exact v_c by almost a factor of 2. In fact, the difference between the exact v_c and zero, corresponding to the complete neglect of the correlation potential, is smaller than the difference between the exact v_c and v_c^{MP2} (for a given density). In other words, starting from the exact KS ground-state density, a single iteration with the EXX-MP2 potential will drive the density further away from the exact starting point than the application of the pure EXX potential. As a consequence, the self-consistent iteration of v_c^{MP2} necessarily increases the deviation of v_c^{MP2} from the exact v_c, as compared to a self-consistent iteration with the correlation potential neglected in the total v_s.

This effect is also visible in the KS excitation energies, which can be regarded as the zeroth-order approximation to the true excitation energies. They are also necessary ingredients of the time-dependent DFT calculations.[47] Selected KS excitation energies for Ne obtained from different KS potentials are collected in Table IV (the LDA and GGA, due to the wrong asymptotic behavior of their exchange potentials, cannot reproduce the Rydberg series and are therefore not included here). Consistent with Fig. 10, the KS excitation energies from the self-consistent EXX potential are more accurate than those from the self-consistent EXX-MP2 calculation. Moreover, as indicated above, already a single application of v_c^{MP2} deteriorates the total potential: This is illustrated in Table IV by the KS excitation energies obtained

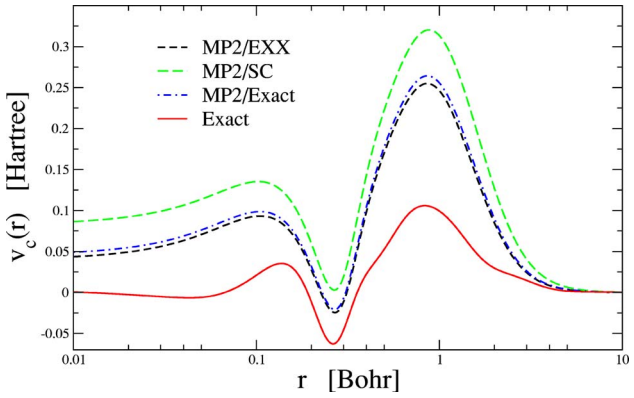

FIG. 10. (Color online) Self-consistent MP2 correlation potential of Ne compared to the v_c^{MP2} obtained from EXX density and from exact KS density. As a reference, the exact correlation potential is also plotted.

TABLE IV. KS excitation energies (in hartree) of neon obtained as differences between occupied and unoccupied KS eigenenergies obtained by self-consistent calculations with different XC functionals.

Excitation	EXX	EXX-MP2	EXX-MP2/EXX	Exact
$1s\rightarrow 3s$	30.628	30.591	30.589	30.633
$1s\rightarrow 3p$	30.706	30.652	30.655	30.706
$1s\rightarrow 3d$	30.762	30.699	30.704	30.759
$1s\rightarrow 4s$	30.748	30.688	30.693	30.746
$1s\rightarrow 4p$	30.769	30.706	30.711	30.766
$2s\rightarrow 3s$	1.526	1.336	1.345	1.469
$2s\rightarrow 3p$	1.604	1.398	1.411	1.542
$2s\rightarrow 3d$	1.661	1.444	1.461	1.595
$2s\rightarrow 4s$	1.646	1.434	1.449	1.582
$2s\rightarrow 4p$	1.667	1.452	1.468	1.602
$2p\rightarrow 3s$	0.659	0.492	0.501	0.612
$2p\rightarrow 3p$	0.736	0.553	0.567	0.684
$2p\rightarrow 3d$	0.793	0.600	0.616	0.738
$2p\rightarrow 4s$	0.779	0.590	0.605	0.725
$2p\rightarrow 4p$	0.799	0.608	0.623	0.744
MAE	0.019	0.079	0.073	

from the combination of the self-consistent EXX potential with the perturbative v_c^{MP2} resulting from the EXX ground state (denoted as EXX-MP2/EXX). The mechanism responsible for this effect is most clearly extracted for the beryllium atom.

C. Instability for beryllium atom

As already indicated, the self-consistent application of the EXX-MP2 functional failed for beryllium. In order to understand this result it is most instructive to analyze the HOMO-LUMO gap, as a vanishing gap lets E_c^{MP2} diverge. This variational instability is particularly likely to show up in systems with a small HOMO-LUMO gap, so that Be is a prime candidate for the instability. The HOMO-LUMO gap for Be is illustrated in Fig. 11(a), where the evolution of the HOMO ($2s$) and LUMO ($2p$) eigenvalues as a function of the number of self-consistent iterations is plotted: The HOMO-LUMO gap decreases gradually and finally breaks down after 16 iterations. This kind of instability is observed no matter what initial guess is used for the SC iteration, indicating that it is an intrinsic behavior of the EXX-MP2 functional in the case of the Be atom. In order to analyze the mechanism which induces the closing of the HOMO-LUMO gap in more detail, v_c^{MP2} as well as the HOMO and LUMO radial orbitals after the 1st, 5th, 10th, and 15th iterations are plotted in Figs. 11(b) and 11(c). The most prominent feature in v_c^{MP2} is that, while the form of the shell structure of v_c^{MP2} remains essentially unchanged during the iterations, its magnitude increases quickly: In the beginning v_c^{MP2} is one order of magnitude smaller than v_x, while after 15 iterations it becomes even larger than v_x. In this way v_c^{MP2} becomes gradually more and more attractive for $r \lesssim 1$ bohr, while a repulsive barrier builds up for $r \gtrsim 1$ bohr. Driven by this change of the correlation potential, the LUMO orbital is pushed inward, so that it experiences more and more the attractive v_c^{MP2} in the region $r < 1$ bohr. The HOMO orbital, on the other hand, is much more stable against variation of v_c. Clearly, any change of the HOMO orbital also affects the dominant components of the energy and thus the potential. However, the minimum of the total EXX energy is obtained with the EXX orbitals, which introduces a restoring force preventing rapid changes of the HOMO orbital. In contrast, the LUMO orbital does not affect the total EXX energy, so that it can be freely modified in order to minimize E_c^{MP2} (which is most easily achieved by reducing the HOMO-LUMO gap). As a consequence, the LUMO eigenenergy can decrease without an analogous response of the HOMO state. The different sensitivities of HOMO and LUMO wave functions to the MP2 potential result in a decreasing HOMO-LUMO gap, which in turn enhances the amplitudes of v_c^{MP2}, finally causing a breakdown of the SC iteration.

Moreover, as Fig. 11(a) shows, the HOMO-LUMO gap decreases monotonically, i.e., it shrinks for each single iteration. This reflects the fact that the shell amplitudes in v_c^{MP2} increase within each single iteration, so that the mechanism which leads to the variational breakdown in the case of beryllium is also responsible for the self-consistency effects observed for stable atoms in Secs. VI A and VI B.

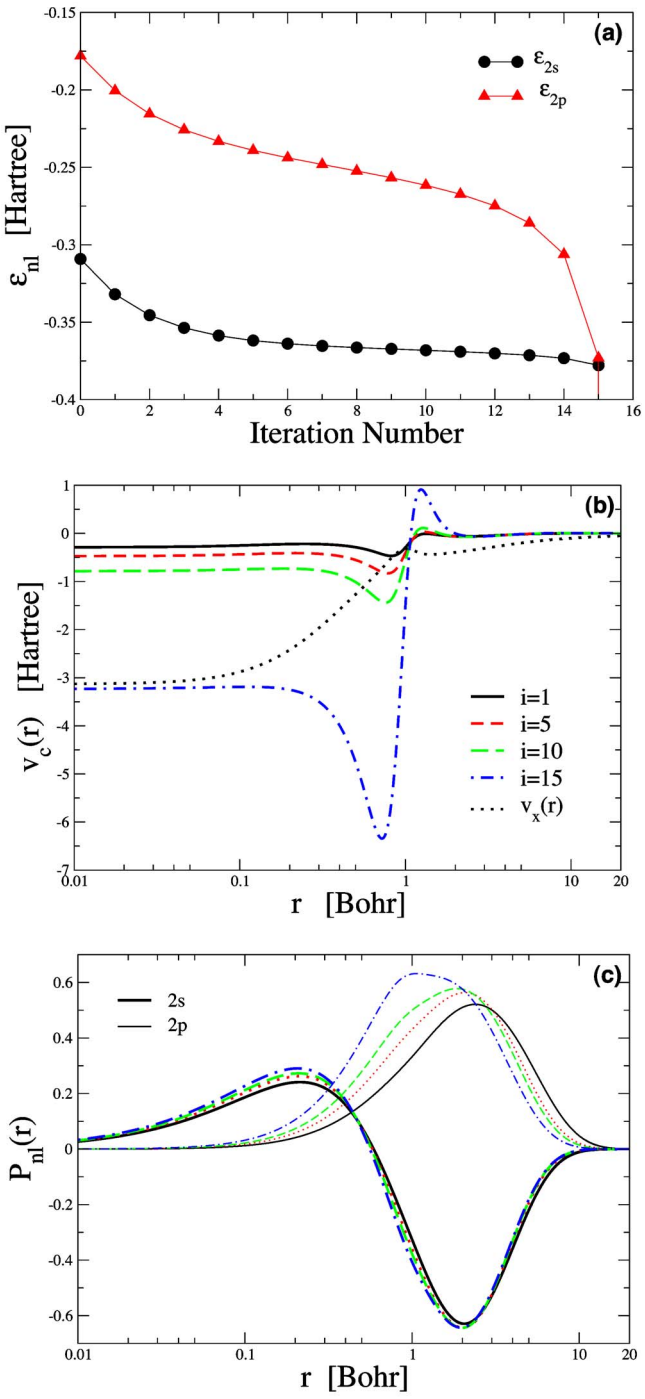

FIG. 11. (Color online) Failure of the MP2-OPM self-consistency procedure for the beryllium atom. (a) Evolution of the HOMO-LUMO gap during the self-consistent iteration. (b) v_c^{MP2} after 1 (solid), 5 (short dash), 10 (long dash), and 15 (dash dot) iterations. As a reference, the exchange potential is also plotted (dot). (c) HOMO ($2s$, thick line) and LUMO ($2p$, thin line) radial orbitals after 1 (solid), 5 (short dash), 10 (long dash), and 15 (dash dot) iterations. The self-consistent EXX KS potential was used as initial guess for starting the iteration.

In Ref. 29, Mori-Sanchez *et al.* report that the self-consistent application of the second-order correlation functional including both single ($E_c^{\Delta\mathrm{HF}}$) and double (E_c^{MP2}) excitations converges to unphysically low total energies for most systems beyond two-electron atoms and small molecules. They attribute this failure mainly to the instability of the single-excitation term. Moreover, Mori-Sanchez *et al.* ob-

tained converged self-consistent results for the beryllium atom, when including only the MP2 term. This apparent discrepancy between our result and that of Mori-Sanchez *et al.* can only originate from the fact that in the work of Mori-Sanchez *et al.*, the KS potential is expanded in terms of a local basis set: The form and size of the basis set restrict the space that the correlation potential can access and can therefore mask the intrinsic instability of the system. In contrast, the present results are based on a numerically exact treatment of both the KS and the OPM equations, without any restriction on the form of the correlation potential. This allows for very narrow structures in v_c^{MP2} as they occur in the case of beryllium [see Fig. 11(b)]. This explanation is consistent with the fact that Mori-Sanchez *et al.* also observed cases in which E_c^{MP2} led to a variational breakdown, both for atoms and molecules.

VII. CONCLUSIONS AND DISCUSSIONS

In this work we have investigated the MP2 correlation potential for atoms in a spherical cavity. Hard-wall boundary conditions have been applied on the surface of the cavity, which ensures a discrete KS spectrum and thus the solubility of the OPM equation. In order to simulate free atoms, the radius of the cavity has been chosen so large that the ground-state density and thus all ground-state observables remain unaffected. We have explicitly verified this latter statement by a comparison of the MP2 correlation energies of atoms in the cavity with those obtained for free atoms. Our results suggest that the cavity approach quite generally can serve as a tool for the self-consistent application of MP2-type functionals to finite systems, if one aims at basis-set-free results.

The success of this scheme relies on the exponential decay of the OPM inhomogeneity over a substantial range of semiasymptotic r values. It seems worthwhile to emphasize that this exponential decay is quite difficult to achieve numerically. The use of the numerically exact kernel of the OPM equation and the inclusion of very high-energy virtual states in the inhomogeneity are instrumental to shift the unavoidable saturation of the inhomogeneity to sufficiently large-r values. Once a sufficiently large virtual space is employed, the incompleteness of the numerical KS spectrum affects the direct solution of the OPM equation only in the chemically irrelevant large-r region: One finds an artificial oscillatory structure which can be removed by a post-treatment of v_c^{MP2} without modifying the behavior of v_c^{MP2} in the chemically relevant region.

Using these techniques, we have determined the numerically exact second-order correlation potentials, free of any basis-set limitations, for a number of prototype atoms. The results offer a mixture of promise and disappointment. On one hand, v_c^{MP2} shows all the features observed for the exact v_c, both for spin-saturated and for spin-polarized systems. In addition to the shell structure reported in previous applications,[28,29,31] v_c^{MP2} also reproduces the coupling between the two spin channels in the case of spin-polarized systems. As neither of these properties is incorporated in LDA or GGA correlation potentials, the results for v_c^{MP2} indicate the scientific potential of implicit density functionals.

On the other hand, the amplitudes of the shell oscillation in the exact v_c are substantially overestimated by v_c^{MP2}, so that the quality of the total KS potential constructed from the exact exchange plus MP2 correlation is worse than that of the exchange-only KS potential. What is more, the MP2 functional is not variationally stable for some systems such as the beryllium atom. It is therefore obvious that the MP2 functional in its original form is not suitable as an orbital-dependent correlation functional for use with the exact exchange. However, as the most basic implicit correlation functional, E_c^{MP2} can serve as a starting point for further development of both refined first-principles functionals (such as the random phase approximation[48–50]) and semiempirical forms (as the ISI approximation[51]). For all these purposes, a thorough understanding of the properties of the second-order correlation functional is essential, and our work provides benchmark results for further developments along these lines.

Atomic systems provide a perfect test bed for developing and analyzing implicit functionals, as their simplicity allows for a highly accurate numerical treatment. The findings for these simple systems can also have important implications for the application of implicit functionals to more complex systems, where usually some basis set, either plane waves or local atomic-type orbitals, is employed. For instance, our results demonstrate the importance of using an extremely accurate kernel for solving the OPM equation, which is consistent with previous findings in the exchange-only case.[52] This point deserves some attention as in most molecular or solid-state calculations, the kernel is calculated by the sum-over-states method, whose accuracy is restricted by the number of orbitals accessible. One possible way to circumvent this bottleneck is the use of numerical approaches in which the OPM problem is solved without inversion of the kernel. Yang and Wu developed a direct minimization method for the OPM problem,[53] in which the KS potential is constructed as a sum of a fixed potential and a linear combination of basis functions, whose coefficients are determined by optimization methods instead of inversion of the integral OPM equation. One important advantage of this method is that it is easy to implement in standard Gaussian orbital-based quantum-chemistry packages. Another promising approach is based on the orbital shift formulation of the OPM problem,[54] in which the OPM integral equation is converted to a nonlinear differential equation of the orbital shifts, so that not even an explicit construction of the kernel is needed. This method has been proven to work well for the exchange-only OPM, but its stability for MP2-type orbital-dependent functionals remains to be examined.

ACKNOWLEDGMENTS

Financial support by the Deutsche Forschungsgemeinschaft (Grant No. EN 265/4-1) is gratefully acknowledged. The calculations for this work have been performed on the computer cluster of the Center for Scientific Computing at the J. W. Goethe-Universität Frankfurt.

[1] P. Hohenberg and W. Kohn, Phys. Rev. **136**, 864 (1964).
[2] W. Kohn and L. J. Sham, Phys. Rev. **140**, 1133 (1965).

[3] R. G. Parr and W. Yang, *Density-Functional Theory of Atoms and Molecules* (Oxford University Press, New York, 1989).
[4] R. M. Dreizler and E. K. U. Gross, *Density Functional Theory: An Approach to the Quantum Many-Body Problem* (Springer-Verlag, Berlin, 1990).
[5] *A Primer in Density Functional Theory*, edited by C. Fiolhais, M. Marques, and F. Nogeira (Springer, Berlin, 2003).
[6] R. M. Martin, *Electronic Structure* (Cambridge University Press, Cambridge, UK, 2004).
[7] J. P. Perdew and S. Kurth, in *A Primer in Density Functional Theory*, edited by C. Fiohais, F. Nogueira, and M. Marques (Springer, Berlin, 2003), Chap. 1, pp. 1–55.
[8] J. P. Perdew and A. Zunger, Phys. Rev. B **23**, 5048 (1981).
[9] E. Engel, A. Höck, and R. M. Dreizler, Phys. Rev. A **61**, 032502 (2000).
[10] K. Terakura, T. Oguchi, A. R. Williams, and J. Kübler, Phys. Rev. B **30**, 4734 (1984).
[11] V. Sahni, J. Gruenebaum, and J. P. Perdew, Phys. Rev. B **26**, 4371 (1982).
[12] D. C. Langreth and M. J. Mehl, Phys. Rev. B **28**, 1809 (1983).
[13] L. J. Sham, Phys. Rev. B **32**, 3876 (1985).
[14] J. B. Krieger, Y. Li, and G. J. Iafrate, Phys. Lett. A **146**, 256 (1990).
[15] E. Engel and S. H. Vosko, Phys. Rev. A **47**, 2800 (1993).
[16] A. Görling and M. Levy, Phys. Rev. A **50**, 196 (1994).
[17] E. Engel and R. M. Dreizler, J. Comput. Chem. **20**, 31 (1999).
[18] T. Grabo, T. Kreibich, S. Kurth, and E. K. U. Gross, in *Strong Coulomb Correlations in Electronic Structure Calculations: Beyond the Local Density Approximation*, edited by V. I. Anisimov (Gordon and Breach, New York, 1999), p. 203.
[19] E. Engel, in *A Primer in Density Functional Theory*, edited by C. Fiohais, F. Nogueira, and M. Marques (Springer, Berlin, 2003), Chap. 2, pp. 56–143.
[20] R. J. Bartlett, V. F. Lotrich, and I. V. Schweigert, J. Chem. Phys. **123**, 062205 (2005).
[21] A. Görling, J. Chem. Phys. **123**, 062203 (2005).
[22] E. J. Baerends, J. Chem. Phys. **123**, 062202 (2005).
[23] J. D. Talman and W. F. Shadwick, Phys. Rev. A **14**, 36 (1976).
[24] Y. Li, J. B. Krieger, and G. J. Iafrate, Chem. Phys. Lett. **191**, 38 (1992).
[25] R. Colle and O. Salvetti, Theor. Chim. Acta **37**, 329 (1975).
[26] T. Grabo and E. K. U. Gross, Chem. Phys. Lett. **240**, 141 (1995).
[27] E. Engel, A. F. Bonetti, S. Keller, I. Andrejkovics, and R. M. Dreizler, Phys. Rev. A **58**, 964 (1998).
[28] I. Grabowski, S. Hirata, S. Ivanov, and R. J. Bartlett, J. Chem. Phys. **116**, 4415 (2002).
[29] P. Mori-Sanchez, Q. Wu, and W. Yang, J. Chem. Phys. **123**, 062204 (2005).
[30] C. Møller and M. S. Plesset, Phys. Rev. **46**, 618 (1934).
[31] A. Facco Bonetti, E. Engel, R. N. Schmid, and R. M. Dreizler, Phys. Rev. Lett. **86**, 2241 (2001).
[32] Y. M. Niquet, M. Fuchs, and X. Gonze, J. Chem. Phys. **118**, 9504 (2003).
[33] H. P. Kelly, Phys. Rev. **131**, 684 (1963).
[34] E. Engel, H. Jiang, and A. Facco Bonetti, Phys. Rev. A **72**, (2005).
[35] C. J. Umrigar and X. Gonze, Phys. Rev. A **50**, 3827 (1994).
[36] M. E. Rose, *Angular Momentum in Quantum Mechanics* (Princeton University Press, Princeton, NJ, 1957).
[37] C. F. Fischer, *The Hartree-Fock Method for Atoms* (Wiley, New York, 1977).
[38] W. H. Press, B. P. Flannery, S. A. Teukolsky, and W. T. Vetterlin, *Numerical Recipes: The Art of Scientific Computing* (Cambridge University, Cambridge, 1989).
[39] J. P. Perdew, J. A. Chevary, S. H. Vosko, K. A. Jackson, M. R. Pederson, D. J. Singh, and C. Fiolhais, Phys. Rev. B **46**, 6671 (1992).
[40] J. Chen, J. B. Krieger, R. O. Esquivel, M. J. Stott, and G. J. Iafrate, Phys. Rev. A **54**, 1910 (1996).
[41] S. H. Vosko, L. Wilk, and M. Nusair, Can. J. Phys. **58**, 100 (1980).
[42] C. Lee, W. Yang, and R. G. Parr, Phys. Rev. B **37**, 785 (1988).
[43] J. P. Perdew, K. Burke, and M. Ernzerhof, Phys. Rev. Lett. **77**, 3865 (1997).
[44] J. Chen and M. J. Stott, Phys. Lett. A **176**, 101 (1993).
[45] C.-O. Almbladh and U. von Barth, Phys. Rev. B **31**, 3231 (1985).
[46] A. D. Becke, Phys. Rev. A **38**, 3098 (1988).
[47] E. K. U. Gross, J. F. Dobson, and M. Petersilka, in *Density Functional Theory II*, Topics in Current Chemistry, Vol. 181, edited by R. F. Nalewajski (Springer, Berlin, 1996), p. 81.
[48] T. Kotani, J. Phys.: Condens. Matter **10**, 9241 (1998).
[49] E. Engel and A. F. Bonetti, Int. J. Mod. Phys. B **15**, 1703 (2001).
[50] F. Furche, Phys. Rev. B **64**, 195120 (2001).
[51] M. Seidl, J. P. Perdew, and S. Kurth, Phys. Rev. Lett. **84**, 5070 (2000).
[52] S. Hirata, S. Ivanov, I. Grabowski, R. J. Bartlett, K. Burke, and J. D. Talman, J. Chem. Phys. **115**, 1635 (2001).
[53] W. Yang and Q. Wu, Phys. Rev. Lett. **89**, 143002 (2002).
[54] S. Kümmel and J. P. Perdew, Phys. Rev. Lett. **90**, 043004 (2003).